

This document is the unedited Author's version of a Submitted Work that was subsequently accepted for publication in ACS Sensors, copyright © American Chemical Society after peer review. To access the final edited and published work see <https://pubs.acs.org/doi/10.1021/acssensors.0c00507>. Access to this work was provided by the University of Maryland, Baltimore County (UMBC) ScholarWorks@UMBC digital repository on the Maryland Shared Open Access (MD-SOAR) platform.

Please provide feedback

Please support the ScholarWorks@UMBC repository by emailing [scholarworks-group@umbc.edu](mailto:scholarworks-group@umbc.edu) and telling us what having access to this work means to you and why it's important to you. Thank you.

## **3D-Printed Microfluidic Devices for Enhanced Online Sampling and Direct Optical Measurements**

Giraso Keza Monia Kabandana, Curtis G. Jones, Sahra Khan Sharifi, and Chengpeng Chen\*

\*Corresponding to:

Dr. Chengpeng Chen  
Department of Chemistry and Biochemistry  
University of Maryland Baltimore County  
Baltimore, MD, USA, 21250  
[cpchen@umbc.edu](mailto:cpchen@umbc.edu)  
+1-4104553053

## INTRODUCTION

Eighty percent of infections result from microbial biofilms<sup>1</sup>. In a biofilm phenotype, bacteria are more prone to be antibiotic resistant compared to planktonic bacteria<sup>2</sup>. Quorum sensing is a widely accepted mechanism for the development of antibiotic resistance, where small extracellular molecules regulate key bioprocesses on the whole-biofilm level<sup>3</sup>. In recent years, Indole produced in high concentrations (millimolar) from tryptophan decomposition by tryptophanase (TnaA)<sup>4</sup>, was identified as a potential quorum sensing molecule<sup>5</sup>. Various studies suggest that indole may play roles in regulating biochemical processes including biofilm formation<sup>6</sup>, antibiotic resistance<sup>7</sup>, and virulence<sup>8</sup>, etc. To further investigate the roles of indole, it is critical to understand the release kinetics of the molecule from a biofilm, a topic that has been difficult to investigate likely due to the lack of a suitable analytical tool.

To study an unknown biochemical process such as indole release, a continuous assay with (near) real-time measurements is more optimal than an end-point detection. In addition to labor-intensity, end-point assays have limited temporal resolution, which may miss unexpected cellular events<sup>9</sup>. Microfluidics provides an ideal platform for continuous quantitation due to its flow-based nature and low sample consumption<sup>10,11,12</sup>. It traditionally applies soft lithography using polydimethylsiloxane (PDMS)<sup>13</sup> to fabricate microfluidic devices. However, 3D-printing recently becomes an alternative methodology<sup>14</sup> due to its unique advantages: 1) 3D-printing enables massive/high throughput production of many devices in one fabrication, and thus quicker prototyping for design optimization (e.g. dimensions)<sup>15</sup>; 2) 3D-printing allows for one-step fabrication of complicated structures. For instance, standard threads have been achieved on 3D-printed microfluidics for robust tubing connection via finger tight adaptors, which is not practical on PDMS-based devices<sup>16</sup>; and 3) 3D-printing can better facilitate technology sharing. Compared to softlithography, which requires multiple dexterous steps to make a device, 3D-printing only requires CAD (computer aided design) files for the fabrication—standard CAD files can be easily shared to promote technology translation<sup>15</sup>.

Nonetheless, compared to PDMS devices, a drawback of 3D-printed microfluidics for analytical applications is the low transparency<sup>15,17</sup>—there has not been a report showing direct

optical measurements through a 3D-printed device. This issue excludes the vast potential to integrate optical detectors on 3D-printed microfluidics for lab-on-a-chip applications. Here we report our finding that, by optimizing the printing orientation, a part can be printed with sufficient transparency for optical measurements. Thus, we fabricated a flow-based detector applying this principle, which showed satisfactory analytical merits. To our knowledge this is the first successful attempt to tune the transparency of a 3D-printed device without additional instruments, materials, and/or protocols, which opens the possibility for directly printing optical components/devices. Coupling the detector device, we also designed a novel microdialysis device. It contains micropillars to enhance flow turbulence for indole sampling from biofilms, enabling higher flow rates and increased dialysis efficiency compared to commercial probes. We successfully applied the microdialysis device connected to the optical detector to measure the kinetics of indole release from biofilms.

## **EXPERIMENTAL**

### **Chemicals and materials**

Indole, p-dimethylaminobenzaldehyde (DMAB), amyl alcohol, hydrochloric acid (HCl), sodium chloride (NaCl), and LB (Luria-Bertani) broth were purchased from Millipore-Sigma (MO, US), and used as received. Ethanol, isopropanol, Hoechst 33258 pentahydrate, and LIVE/DEAD® BacLight™ bacterial viability kit were purchased from Thermo Fisher Scientific (MA, US). Polycarbonate membrane with 50 nm pore size was from Whatman (PA, US). All flow connectors and tubing were from Cole-Parmer (IL, US). Microfluidic syringe pumps were obtained from New Era (NJ, US). The modular spectrometers and optical fibers were purchased from BWTek (DL, US).

### **Kovac's reagent optimization**

The conventional Kovac's reagent made by dissolving 5% DMAB in amyl alcohol/HCl (3/1 v/v) was not optimal for quantitation. To optimize the assay, we prepared different concentrations (2.5, 5, and 10%) of DMAB in different alcohol solvents (ethanol, isopropanol, and

amyl alcohol) and assessed the analytical merits of the various combinations in measuring indole standards (**Figs. S1A** and **S1B** in the SI).

### **3D printing of the devices**

All the microfluidic devices were designed in the software of Autodesk Inventor (CA, US) and printed by our 3D printer (Projet MJP 5600; 3D Systems, SC, US) in high-resolution mode (x,y resolution=33  $\mu\text{m}$ , z resolution=13  $\mu\text{m}$ ). The VisiJet CR-CL 200 material was used, which is propriety in terms of composition but is acylate-based. Wax (Visijet S500) was used as the support material, which can melt and thus be removed in a 75°C oven. The design and dimension details of the devices were attached in the SI (**Figs. S2A** and **S2B** in the SI).

### **Membrane attachment to the dialysis probe**

The dialysis device was printed with an open channel, where a piece of porous membrane was attached to enclose the channel. To attach the membrane, a thin layer of super glue was applied to the device and after 10 minutes, the membrane (polycarbonate; 50 nm pore size) was directly attached to it and set for 24 hours to completely cure at room temperature. The dialysis probe was hanging in a petri dish through a fitting hole on the lid without touching the agar layer (**Figs. S2C** and **S2D** in the SI).

### **Device transparency measurements**

Optical fibers were aligned with or without a device in between. The intensity of light between 400 and 800 nm was detected at 1nm intervals. The detected intensity without a device were normalized to 100%. With a device, the percentage of transmitted light was then calculated.

### **Setting up the quantitation system**

**Fig. 1** and **Fig. 4B** show the illustration and the real setup of the system. Microbore Tygon tubing (0.02"ID, 0.06"OD) was used to connect the microdialysis device, a T-mixer, and the microfluidic detector, through which, a dialysis buffer (1% w/v NaCl, the salt composition of LB

media) was perfused. Kovac's reagent was pumped into the remaining arm of the T-mixer to be mixed with the dialysate before entering the microfluidic detector.

Optical fibers were inserted into the matching holders at both ends of the light pass channel in the detector device for absorbance detection. A tungsten lamp was used as the incident light and the transmittance light was conducted via the second optical fiber to a modular spectrometer. Absorbance at 570 nm ( $\lambda_{\text{max}}$  of the indole-Kovac's product) and 600 nm (reference  $\lambda$  to calibrate any possible baseline drifting) were detected every 20 sec in the software of the spectrometer. The ( $\text{Abs}_{570} - \text{Abs}_{600}$ ) was used as the signal intensity.

To characterize the analytical merits of the system, indole standards of 0, 50, 100, 150, 200, 250, and 300  $\mu\text{M}$  were prepared in LB broth and were added to agar petri dishes without a biofilm. The microdialysis device was then placed in the dishes from low to high concentrations, followed by continuous absorbance measurements for  $\sim 10$  min of each concentration. The detected signals were averaged and plotted as a function of the concentrations.

### **Bacteria culture**

*Escherichia coli* (*E. coli*) strain W-3104 was purchased from ATCC (VA, US). The *E. coli* cells were inoculated in 10 mL LB media and incubated overnight in a humid incubator at 37 °C. The overnight *E. coli* solution was added to 80% glycerol in 1:1 ratio and frozen as a stock in a liquid nitrogen tank. Prior to biofilm culture, an inoculator was used to scratch the surface of the frozen *E. coli* and suspended in 10 mL LB broth in a sterile biohood. After an overnight incubation at 37 °C, an aliquot of 1 mL of the cell culture was uniformly distributed onto 1% (w/v) agar plates and the supernatant was removed after 30 seconds. Following the well-established protocol by Ray and colleagues<sup>18</sup>, the plates were incubated for 72 hours in a humid incubator at 37 °C to allow the formation of mature biofilms. The agar plates were prepared by dissolving 1% (w/v) agar powder in the LB broth followed by autoclaving, and immediately adding 5 mL of the agar solution to a 60 mm sterile petri dish.

### **Fluorescent imaging of W-3104 biofilms**

A mature biofilm grown for 72 hours in a 37 °C incubator was stained with a live/dead bacterial viability assay. An aliquot of 3 µL of SYTO® and propidium iodide were added to 1 mL of PBS, respectively. The solution was then added to the biofilm in a petri dish from the side to avoid cell detachment from the surface. This was followed by an incubation in the dark for 15 minutes at room temperature. The dye solution was then removed, and the biofilm was washed four times with sterile PBS before imaging.

### **Quantitation of biofilm-induced indole**

To quantitate indole release from biofilms, a control and an experimental group were conducted simultaneously under the same environment. The control contained 5 mL of LB broth above the biofilm in a petri dish (60 mm diameter) while the experimental group contained 0.1 µg/mL of levofloxacin (10% of the minimal inhibitory concentration which does not affect cell proliferation) in 5mL LB broth. The two petri dishes were placed in a humid box at room temperature. The dialysate from each petri dish flowed to the microfluidic detector device after being mixed with the optimized Kovac's reagent in a T mixer, followed by absorbance measurements for 24 hours with 20-sec intervals. Although the same amount of *E. coli* cells was seeded in each petri dish, the total number of bacteria after the biofilm was formed might slightly differ, which needed to be normalized. To do that, after an indole measurement, the bacteria in the petri dish were lysed using 1 mL lysis buffer (10% Tris-HCl, pH 7.5; 10% EDTA, pH 8.0; 20 µg/mL lysozyme in MilliQ water), and the gross amount of DNA was quantitated using the Hoeschst 33258 assay<sup>19</sup>. A calibration curve was obtained by lysing various known amounts of bacteria and quantitating the DNA in the lysates.

### **Data analyses and statistics**

The raw time-course absorbance data were exported from the BWTech software (.txt format) to Microsoft Excel. LOD was calculated by multiplying 3 with the standard deviation of the y-intercept of the regression line, and dividing the result by the slope of the calibration curve<sup>20</sup>. With the calibration curve, indole concentration at each time point was calculated. Next, the released indole was normalized by the number of bacteria in each petri dish. Standard

deviation was used as the error bars in the results unless otherwise noted. Student-t test was applied to compare differences; significant difference was considered only when p values are smaller than 0.05.

## **RESULTS AND DISCUSSION**

Although studies reported that extracellular indole can be involved in the development of antibiotic resistance of a biofilm<sup>7</sup>, the secretion kinetics of this molecule had not been known likely due to the lack of a suitable quantitative tool. We present a new design of a microfluidic system that was used for automated and near real-time measurement of indole.

### **An overview of the microfluidic system**

As **Fig. 1** shows, the microfluidic system contains two 3D-printed devices: a microdialysis probe, and a microfluidic optical detector. The dialysis device was placed above a biofilm in a petri dish, so that the secreted indole could be extracted in the flowing buffer. The buffer then mixed with the optimized Kovac's reagent (Figs. **S1A** and **S1B** in the SI) in the mixer and flowed into the detector. Optical fibers coupled to a modular spectrometer were placed across the channel of the device for automated measurements. Both the microdialysis and the microfluidic detector devices are innovative: the micropillar design in the microdialysis channel enhanced flow turbulence and thus extraction efficiency; for the first time, we found that the transparency of a 3D-printed device can be simply tuned by orientation adjustments. Details are elaborated below.

### **The novel microdialysis device**

A microdialysis device is indispensable to measure secreted (extracellular) indole because a biofilm keeps releasing planktonic bacteria to its culture media, which can be easily lysed by the Kovac's reagent to release large amounts of cytoplasmic indole. Therefore, instead of analyzing the media of a biofilm directly (e.g. from supernatant), a separation mechanism to prevent the interference from floating cells is necessary. Compared to common cell separation



techniques such as density centrifugation, it is more practical to integrate a microdialysis device on the system for continuous flow-based sampling, which applies a porous membrane to exclude cells out of the flow stream.

Although commercial capillary-based microdialysis probes are available, they require low perfusion rates ( $<1\ \mu\text{L}/\text{min}$ ) with limited extraction efficiency ( $<1\%$ )<sup>21</sup>. A typical way to utilize a microdialysis is to collect the dialysate for long sampling periods (1-10 min) followed by sample concentrating and analyses<sup>22,23</sup>, making it suboptimal to conduct near real-time measurements. Here, we report a novel 3D-printed microfluidic dialysis scheme, which is sufficiently robust for high flow rates (thus high temporal resolution) yet with enhanced extraction efficiency.

As shown in **Fig. 2A**, the dialysis device was 3D-printed in a circular shape with a serpentine channel ( $400\ \mu\text{m} \times 400\ \mu\text{m}$  cross section;  $400\ \mu\text{m}$  deep) containing micropillars. The concaved open channel was sealed by attaching a piece of porous (50 nm pore size; polycarbonate) membrane, which served as the dialysis structure.

The micropillars ( $200\ \mu\text{m}$  diameter;  $200\ \mu\text{m}$  high; **Fig. 2B**) were designed to increase flow turbulence and thus the extraction/dialysis efficiency. Flow in microchannels is typically laminar with limited mass transfer and mixing<sup>24</sup>. As illustrated in **Fig. 2C**, with a laminar flow in the fluidic channel, the extracted molecules (green dots) are confined within a thin layer next to the membrane until saturation. With random turbulence, however, the molecules can be mixed in a larger volume of liquid and thus resulting in a sharper concentration gradient across the membrane to facilitate further extraction. We simulated and modeled flows going through a channel with or without pillars using Computational Fluidic Dynamics (CFD). As **Fig. 2D** demonstrates, a flow rate can be resolved into three vectors along the x, y and z directions, and the z vector ( $V_z$ , perpendicular to the flow direction) can suggest how turbulent the flow is. Without pillars in the channel, minimal  $V_z$  of  $2\ \mu\text{m}/\text{s}$  was observed. With the micropillars, however, the  $V_z$  increased by 250 folds to  $500\ \mu\text{m}/\text{s}$ . We then modeled the diffusion profiles of indole across the membrane into channels with or without the pillars. **Fig. 2E** shows the results from a cross view of the channels. The “x” symbol means the flow direction is perpendicular to the paper plane towards the inside. The color change is the concentration gradient (500 to  $0\ \mu\text{M}$ , red to blue). The micropillars significantly enlarges the diffusion zone, indicating more extracted

indole molecules in the flow. We further confirmed the simulation results by measuring the dialysis efficiency. The micropillars significantly increased the extraction efficiency by ~3 folds (**Fig. 2F**).

Few papers reported 3D-printed microfluidic dialysis devices<sup>25,26</sup>. Here, we show the feasibility to utilize 3D-printing to fabricate additional microstructures in a microfluidic channel to enhance dialysis efficiency. Compared to conventional soft lithography, which requires multiple steps and/or photomasks to pattern additional microstructures, 3D-printing represents a one-step alternative to include desired microfeatures in microfluidics. The detailed design of our device is available in the SI (**Fig. S2A**), which can be translated to other researchers for continuous sampling from cell cultures.

### **The detector device that allows for direct optical measurements**

The second part of the system is the microfluidic optical detector, where the lysate from the dialysis device was continuously measured. **Fig. 3A** demonstrates the device: the inlet and outlet were designed to fit a standard 10-32 threaded male connector for flow delivery; serpentine channels were designed right after the inlet to further mix the dialysate and the Kovac's reagent; the mixed solution then passed through a straight channel, where light illuminated through and absorbance was detected via optical fibers inserted in the holders. Based on Beer's law<sup>27</sup>, the absorbance intensity is proportional to the length of a light path. Therefore, we optimized the length of the straight channel (equals to light path) by making devices with three dimensions (5, 10, and 20 mm), followed by absorbance measurements of 2  $\mu$ M indole standards. It was found that the 20 mm channel caused high absorbance intensities that overflow the upper detection capacity of our spectrometer. The 5 mm length did not produce as intense signals as from the 10 mm device. Therefore, we chose the devices with a 10 mm straight channel for the absorbance detection.

With a conventional microfluidic device made from PDMS, the typical scheme of on-chip optical detection is to place optical fibers perpendicular to the microfluidic channel<sup>28</sup>, which has limited light pass (height/width of the channel; hundreds of  $\mu$ m) and thus lower sensitivity. Although a few papers reported methods to embed optical fibers in PDMS parallelly to a

microfluidic channel<sup>29,30</sup>, due to the microscale of the features and the difficulty to manually align the two components, these protocols are highly skill-based and not widely translational. 3D-printing can circumvent this issue because rigid structures with precise alignments can be easily fabricated. For our device, two holders that fit optical fibers were printed at both ends of the microfluidic channel, which aligned the centers of the optical fibers and the microchannel precisely for light to pass through. This design provides a simple, reproducible, and robust protocol to include optical fibers on microfluidics.

For optical measurements, in addition to reproducible optical fiber positioning, a bigger concern arises from the transparency of the 3D-printing material. [For poly-jet 3D printers, the manufactures provide relatively transparent materials well-suited for their 3D printers. For our printer, VisiJet CR-CL 200 is the most transparent material available.](#) Although manufacturers claim their materials are “transparent”, 3D-printed parts from these materials are typically translucent and there has not been a literature reporting direct optical measurements through a 3D-printed device<sup>15</sup>. Here, we report our finding that using the same material, the printing orientation affects the transparency of the finished part. With the optimal orientation, we can generate devices that are sufficiently transparent for direct optical detection. **Fig. 3B** illustrates the general principle of a 3D-printing process—a layer material of is added on previous ones in the z direction until all the stacked layers form a 3D shape. For poly-jet 3D printing, a layer of liquid resin is finely spread and cured before the next one is deposited. Due to the layer stacking, it is likely that the sides of a part (such as the one in **Fig. 3B**) are rougher and less transparent. To prove this assumption, we printed the detector device in two orientations and tested light transmittance. In **Fig. 3C**, the optical windows (oval circles) where the light needs to pass through between the optical fibers and the flow, were printed parallel to the xy plane. The inset picture indicates that a light beam could go through. Further transmittance analyses revealed that in the 400-500 nm range, the transmittance was between 55% and 80%; over 500 nm, the transmittance was stabilized above 80%. For the device printed in the orientation shown in **Fig. 3D**, where the optical windows were perpendicular to the xy plane with layer edges built up, visible transmitted light spot could not be observed, and the overall transmittance was only around 10%.

With the more transparent device (**Fig. 3C**), we characterized its analytical merits by directly pumping indole standards and the Kovac's reagent (**Fig. S4A** in the SI) into the device with absorption measurements.

**Fig. S4B** in the SI shows that step increased signals were obtained with increased indole concentrations. By plotting the average signals on each step as a function of the concentrations, a linear calibration curve was generated with the detection limit (LOD) being 0.8  $\mu\text{M}$ , which is within the lowest range (sub  $\mu\text{M}$ ) of UV-vis spectroscopy. This result confirmed that the transparency of the device is enough for optical quantitation.

This is the first time to conduct direct optical measurements on a 3D-printed device. Noteworthy, an 800% increase in light transmittance was achieved simply by adjusting the printing orientation without additional instruments, materials, or protocols. This finding is a significant progression in the field of 3D-printed microfluidics with foreseeable applications such as on-chip detection and imaging. It also opens the possibility to directly 3D-print optical components for sensor development.

### **Apply the system to quantitate the kinetics of indole release from biofilms**

Accumulating evidence indicates that extracellular indole can serve as a signaling molecule between bacteria in a biofilm. To further investigate the effects of indole in a biofilm, we applied our microfluidic system to measure indole release kinetics from an *E. coli* biofilm model, which had not been known.

As shown in **Fig. 4A**, we successfully cultured biofilms on an agar plates following the established protocol<sup>18</sup>. **Figs. S2C** and **S2D** in the SI demonstrate how the dialysis device were hung in the culture media above the biofilm in a petri dish. **Fig. 4B** depicts the setup of the online optical quantitation of biofilm-induced indole. **Parallel** measurements from two petri dishes were conducted simultaneously **using two sets of the devices** such that both the control and the experimental biofilms were measured under the same environment.

The control was an *E. coli* biofilm in normal LB broth while the experimental contained levofloxacin (10% of minimal inhibitory concentration which does not kill the bacteria, **Fig. S5** in the SI). A NaCl solution (1% w/v; the salt component of LB broth) was pumped through the

dialysis device immersed in the petri dish to extract indole. The optimized Kovac's reagent was delivered to a T-mixer to join the dialysate at 12  $\mu\text{L}/\text{min}$  (same flow rate as the dialyzing buffer), which was determined as the optimal flow rate (**Fig. S3** in the SI). It was determined that the T-mixer and the serpentine channel could sufficiently mix the two solutions as indicated by the data in **Fig. S6** in the SI. The optical microfluidic detectors were placed in a dark box conjugated with optical fibers. Two modular spectrometers were linked to the optical fibers, which were set to take measurements every 20 sec for 24 hours.

**Fig. 4C** shows the measurements of indole standards added to empty petri dishes. After averaging the signal intensity on each plateau and plotting it as a function of the concentrations, a linear calibration curve was obtained ( $R^2 = 0.996$ ) with an LOD of 21.2  $\mu\text{M}$ , which is sufficient for quantitating indole release from *E. coli* biofilms, observed in the 200-300  $\mu\text{M}$  range by our end-point measurements.

**Fig. 4D** shows the results of indole release kinetics. Overall, biofilms treated with levofloxacin produced significantly more indole than the untreated ( $10.1 \pm 0.2$  vs.  $4.8 \pm 0.2$  fM/cell;  $p < 0.01$ ). Also, the treated biofilms released indole at a higher rate: within the first 2.5 hours, the rate of indole release with levofloxacin was  $2.32 \pm 0.19$  fM/cell/hr, which was significantly higher than that of the untreated biofilms ( $1.30 \pm 0.01$  fM/cell/hr). The times to reach concentration plateaus also differed: the treated biofilms continued to release indole for  $10.3 \pm 0.7$  hours, whereas the control stopped releasing after  $5.5 \pm 0.1$  hours.

Although all the printed devices could be reused after being thoroughly cleaned, we used a different device each time because the cleaning process was arduous, and many devices could be printed in high throughput. The devices (from the same or different printing batches) did not show significant difference in analytical merits—we did calibration curves on each device and did not see significant difference in terms of sensitivity and signal intensities. Also, due to the high precision and reproducibility of the printer (dimension variance  $< 2\%$ ), and the rigidity of the material, we did not encounter issues when aligning the optical fibers with the detection channels on the microfluidic devices.

Enabled by our microfluidic system, this is the first time to quantitate the release kinetics of indole from a biofilm with and without antibiotic stimulation, which lays a foundation for future research to further study the effects of extracellular indole.

## **CONCLUSION**

We developed an innovative microfluidic system that contains a microdialysis device for continuous sampling and a downstream detector for near real-time quantitation. Both devices are novel. The microdialysis device represents a new dialysis design with micropillars in the channel to promote flow turbulence and thus enhanced extraction efficiency. We also report for the first time that the transparency of a 3D-printed part can be tuned by the printing orientation. Transmission of visible light through our detector device printed with the optimal orientation was sufficiently high (80%) for quantitative optical measurements. This finding shows the feasibility to directly 3D-print optical detectors/components for analytical applications. We successfully applied the system to quantitate the kinetics of indole release from quiescent and stimulated biofilms, a phenomenon that had not been previously known. This new knowledge will benefit future efforts to investigate the roles of extracellular indole in biofilms.

## FIGURES AND CAPTIONS

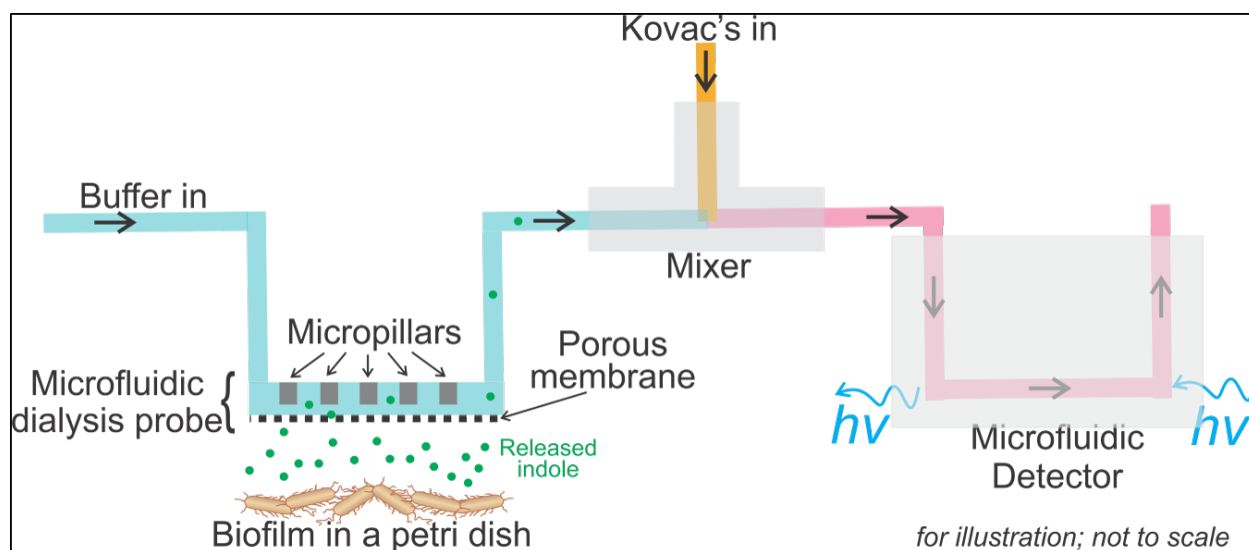


**Figure 1. Illustration of the microfluidic system.** A microfluidic dialysis probe was 3D-printed with micropillars in the flow channel and attached with a porous membrane, which was placed above a biofilm cultured in a petri dish. The flowing dialysis buffer extracted indole molecules released from the biofilm and brought them to a mixer, where the Kovac's reagent was mixed in to react with indole and produce a pink azoic product. The second part of the system is a microfluidic detector, whose transparency was tuned for direct optical measurements.

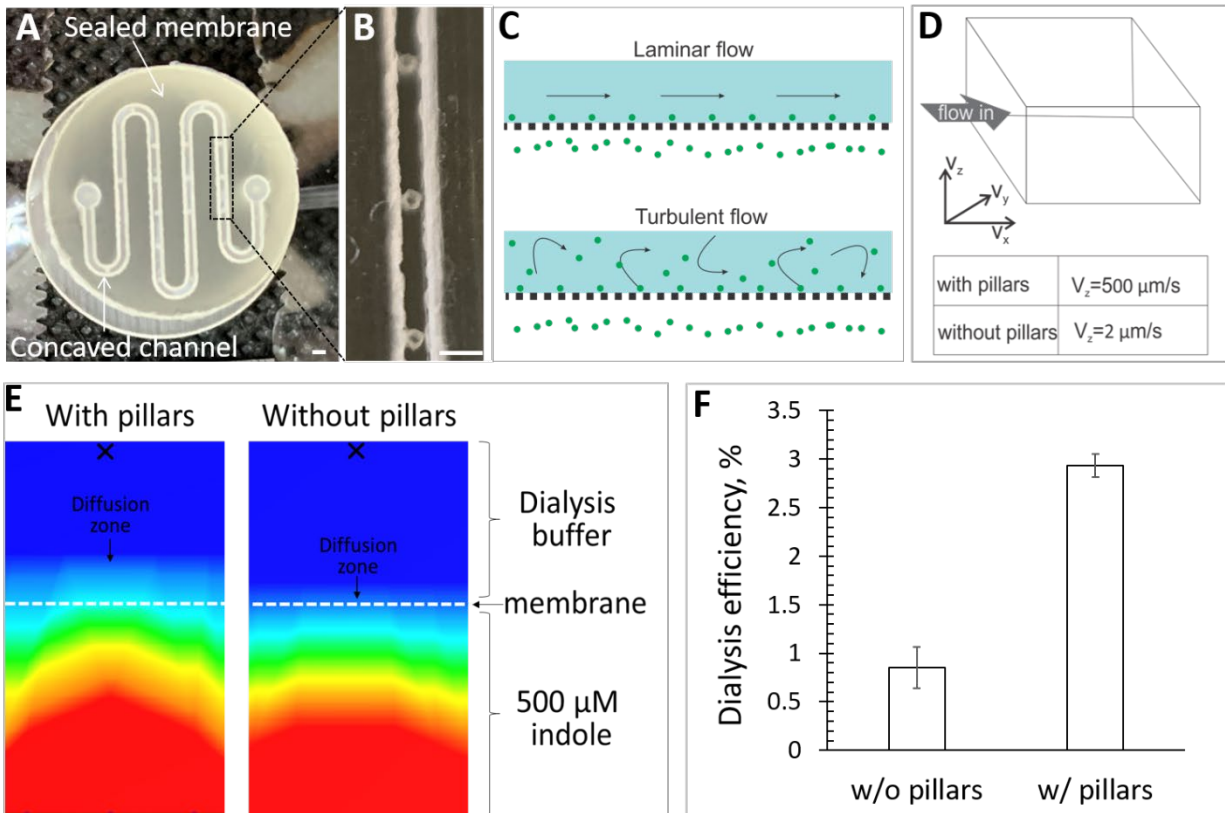


**Figure 2. The design, principle, and characterization of the microdialysis device.** (A) The device was 3D-printed in a disc shape with a concaved serpentine channel. Upon being printed, the channel was open on top. A piece of porous polycarbonate membrane (50 nm pore size) was attached to the top surface to seal the open channel and to serve as the microdialysis structure. The channel was  $400 \mu\text{m} \times 400 \mu\text{m}$  (cross section) and  $400 \mu\text{m}$  deep. Scale bar =  $500 \mu\text{m}$ . (B) Micropillars of  $200 \mu\text{m}$  (diameter and height) were fabricated in the microfluidic channel to increase dialysis efficiency by inducing turbulent flow. Scale bar =  $500 \mu\text{m}$ . (C) With laminar flow in a microfluidic channel, the dialyzed molecules (green dots) saturate in a thin layer close to the porous membrane. A turbulent flow could enhance the dialysis efficiency by introducing the molecules into a larger volume of the buffer. (D) The flow rate into a microfluidic channel can be resolved into x, y, and z vectors.  $V_z$  (perpendicular to the flow direction) is an indicator of flow turbulence. We applied Computational Fluidic Dynamics (CFD) to simulate the flows, finding that with the micropillars in the microfluidic channel, the  $V_z$  vector was 250 folds higher than that in a non-pillar channel. The results suggest that the pillars led to turbulence in the microfluidic channel. (E) Further simulation and modeling show that with the pillars, the diffusion zone of indole was significantly larger on the inner side of the membrane. Pictures are cross views. The “x” sign means flow direction is perpendicular to the paper plane. (F) Experimental results confirmed the simulations: the micropillars significantly increased dialysis efficiency by  $\sim 3$  folds.  $N=3$ , error=stdev,  $p<0.01$ .



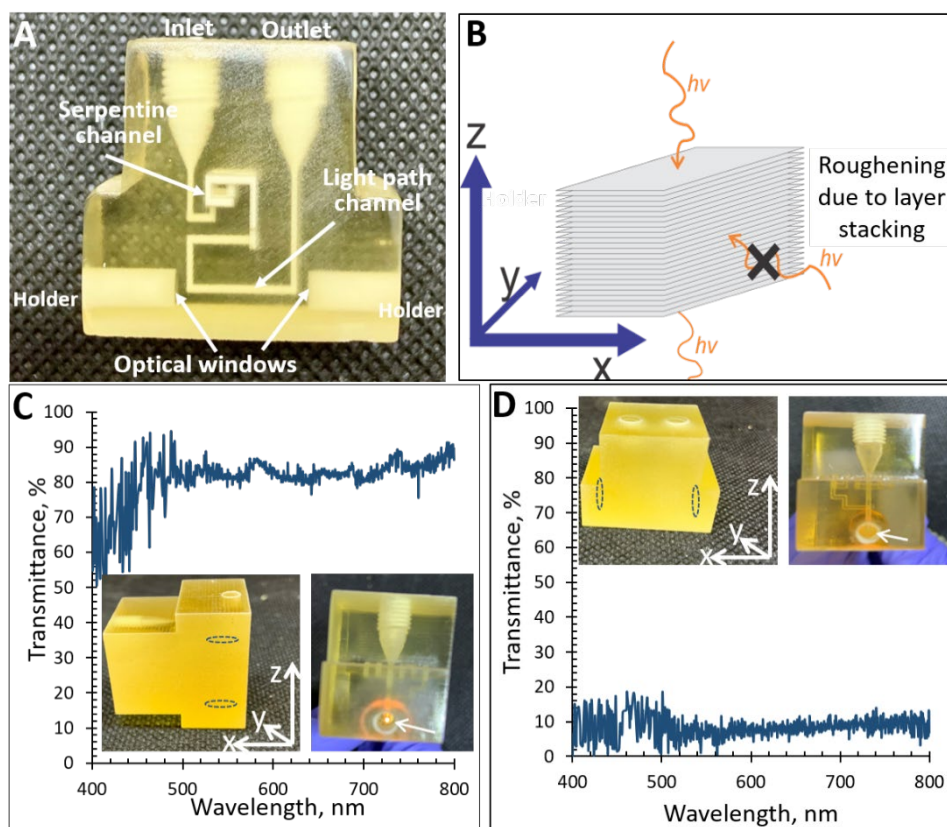


**Figure 3. The optical detection device and the effects of printing orientation on transparency.**

**(A)** The 3D-printed microfluidic optical detector. A sample mixed with Kovac's reagent entered the device via the inlet, which was further mixed by the serpentine channels with right angles. The light path channel was where optical (absorption) detection occurred, on both ends of which, holders that fit optical fibers were designed. The two optical fibers were used for delivering incident light (Tungsten lamp) and for detecting transmitted light, respectively. **(B)** The difference of optical properties on the different sides of a 3D-printed object. 3D printing is achieved by laying thin layers on previous ones along the z direction. Because of the roughness caused by layer stacking on the sides, light cannot go through. However, light can pass through any plane parallel to xy. **(C)** With the microfluidic detector printed with the optical windows (dashed ovals) parallel to the xy plane (printing stage), light beam through the device could be observed (arrow). Transmittance analyses revealed that above 500 nm, over 80% of light could transmit through. **(D)** With the microfluidic detector printed in the orientation where the optical windows were perpendicular to the xy, the light beam could not be seen from the other side of the device. Transmittance was only around 10%.

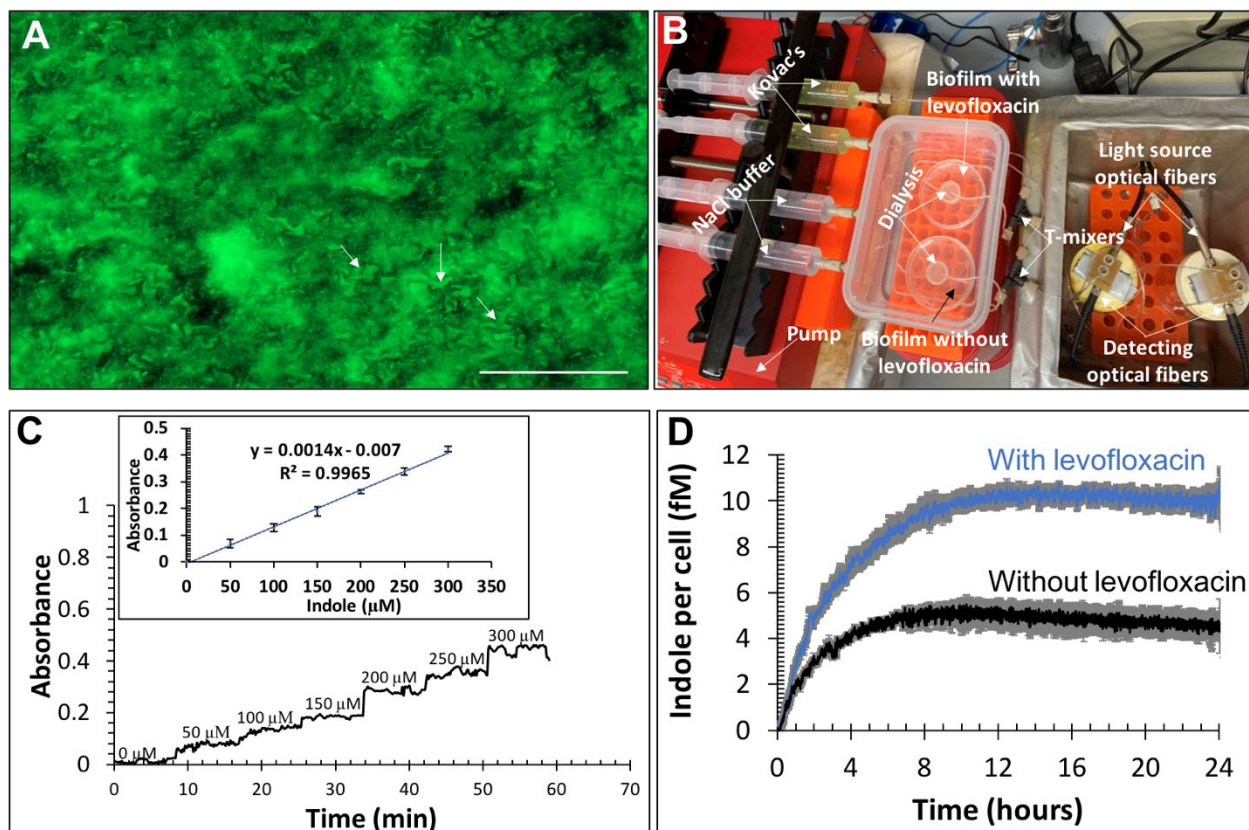


**Figure 4. Using the system to quantitate biofilm-induced indole release. (A)** Fluorescent staining of an *E. coli* W-3104 biofilm. The green area shows the biofilm (DNA stained by SYTO). The arrows point out examples of single bacterium on the top. **(B)** A picture of running the microfluidic system. A control and an experimental group (containing levofloxacin of 10% MIC) were conducted simultaneously. The syringe pumps delivered the dialysis buffer and the Kovac's reagent at 12  $\mu\text{L}/\text{min}$ , which were mixed after the petri dishes in the T-mixers. The mixed solution flowed through the microfluidic detectors for continuous measurements. **(C)** Characterization of the analytical merits of the system. Indole standards were added in petri dishes and detected by the system. Increased absorbance signals were obtained with increased indole concentrations. The calibration curve obtained by plotting the plateau averages versus the standards concentrations showed a linearity with  $R^2=0.9965$  and LOD of 21.2  $\mu\text{M}$ .  $N=3$ , Error=stdev. **(D)** The kinetics of indole release from biofilms treated with or without levofloxacin. Absorbance signals were acquired for 24 hours with 20-sec intervals via the programmed spectrometers, after which, the bacteria in each petri dish were lysed and the gross amount of DNA was quantitated using the Hoechst assay<sup>31</sup> as a measurement of cell numbers. The calibrated indole release was then normalized to per bacterial cell. Biofilms treated with levofloxacin produced significantly more indole than the control ( $10.1 \pm 0.2$  fM/cell vs.  $4.8 \pm 0.2$  fM/cell) after plateau ( $p < 0.01$ ). Also, release kinetics significantly differed in terms of release rate and the time hitting plateau.  $N=5$ , error=S.E.M.

## REFERENCES

- [1] H. Wu, C. Moser, H.Z. Wang, N. Hoiby, Z.J. Song, Strategies for combating bacterial biofilm infections, *International Journal of Oral Science*, **2015**, 7(1), 1-7.
- [2] J.L. Balcázar, J. Subirats, C.M. Borrego, The role of biofilms as environmental reservoirs of antibiotic resistance, *Frontiers In Microbiology*, **2015**, 6 1216-1216.
- [3] J.Y. Sharahi, T. Azimi, A. Shariati, H. Safari, M.K. Tehrani, A. Hashemi, Advanced strategies for combating bacterial biofilms, *Journal of Cellular Physiology*, **2019**, 234(9), 14689-14708.
- [4] N.M. Vega, K.R. Allison, A.N. Samuels, M.S. Klemperer, J.J. Collins, Salmonella typhimurium intercepts Escherichia coli signaling to enhance antibiotic tolerance, *Proceedings of the National Academy of Sciences of the United States of America*, **2013**, 110(35), 14420-14425.
- [5] D.D. Wang, X.D. Ding, P.N. Rather, Indole can act as an extracellular signal in Escherichia coli, *Journal of Bacteriology*, **2001**, 183(14), 4210-4216.
- [6] P. Di Martino, R. Fursy, L. Bret, B. Sundararaju, R.S. Phillips, Indole can act as an extracellular signal to regulate biofilm formation of Escherichia coli and other indole-producing bacteria, *Canadian Journal of Microbiology*, **2003**, 49(7), 443-449.
- [7] Y. Han, Y. Wang, Y.M. Yu, H.T. Chen, Y.M. Shen, L.C. Du, Indole-Induced Reversion of Intrinsic Multiantibiotic Resistance in Lysobacter enzymogenes, *Applied and Environmental Microbiology*, **2017**, 83(17), 14.
- [8] L. Jintae, C. Attila, S.L.G. Cirillo, J.D. Cirillo, T.K. Wood, Indole and 7-hydroxyindole diminish Pseudomonas aeruginosa virulence, *Microbial Biotechnology*, **2009**, 2(1), 75-90.
- [9] K. Vittayarukkul, A.P. Lee, A truly Lego-like modular microfluidics platform, *Journal of Micromechanics and Microengineering*, **2017**, 27(3), 035004.
- [10] S. Subramanian, E.I. Tolstaya, T.E. Winkler, W.E. Bentley, R. Ghodssi, An Integrated Microsystem for Real-Time Detection and Threshold-Activated Treatment of Bacterial Biofilms, *Acs Applied Materials & Interfaces*, **2017**, 9(37), 31362-31371.
- [11] E. Dervisevic, K.L. Tuck, N.H. Voelcker, V.J. Cadarso, Recent Progress in Lab-On-a-Chip Systems for the Monitoring of Metabolites for Mammalian and Microbial Cell Research, *Sensors*, **2019**, 19(22), 36.
- [12] G.M. Whitesides, The origins and the future of microfluidics, *Nature*, **2006**, 442(7101), 368-373.
- [13] M.P. Wolf, G.B. Salieb-Beugelaar, P. Hunziker, PDMS with designer functionalities- Properties, modifications strategies, and applications, *Progress in Polymer Science*, **2018**, 83 97-134.
- [14] C.K. Dixit, K. Kadimisetty, J. Rusling, 3D-printed miniaturized fluidic tools in chemistry and biology, *Trac-Trends in Analytical Chemistry*, **2018**, 106 37-52.
- [15] C.P. Chen, B.T. Mehl, A.S. Munshi, A.D. Townsend, D.M. Spence, R.S. Martin, 3D-printed microfluidic devices: fabrication, advantages and limitations-a mini review, *Analytical Methods*, **2016**, 8(31), 6005-6012.
- [16] C.P. Chen, Y.M. Wang, S.Y. Lockwood, D.M. Spence, 3D-printed fluidic devices enable quantitative evaluation of blood components in modified storage solutions for use in transfusion medicine, *Analyst*, **2014**, 139(13), 3219-3226.
- [17] S. Waheed, J.M. Cabot, N.P. Macdonald, T. Lewis, R.M. Guijt, B. Paull, M.C. Breadmore, 3D printed microfluidic devices: enablers and barriers, *Lab on a Chip*, **2016**, 16(11), 1993-2013.

- [18] V.A. Ray, A.R. Morris, K.L. Visick, A Semi-quantitative Approach to Assess Biofilm Formation Using Wrinkled Colony Development, *Jove-Journal of Visualized Experiments*, **2012**, (64).
- [19] N.L. Vekshin, A.N. Doynikova, A.M. Lvov, Determination of Micro-Quantities of DNA Using DNase and Fluorescence of Hoechst 33258 and Light-Scattering, *Journal of Fluorescence*, **2019**, 29(2), 479-484.
- [20] K.A. Tuwei, N.H. Williams, M. Grell, Fibre optic absorbance meter with low limit of detection for waterborne cations, *Sensors and Actuators B-Chemical*, **2016**, 237 1102-1107.
- [21] M. Konig, A. Thinnies, J. Klein, Microdialysis and its use in behavioural studies: Focus on acetylcholine, *Journal of Neuroscience Methods*, **2018**, 300 206-215.
- [22] K.N. Schlitz, R.T. Kennedy, Time-Resolved Microdialysis for In Vivo Neurochemical Measurements and Other Applications, *Annual Review of Analytical Chemistry*, Annual Reviews, Palo Alto, 2008, pp. 627-661.
- [23] M. Carter, J. Shieh, Chapter3 Stereotaxic Surgeries and In Vivo Techniques, *Guide to Research Techniques in Neuroscience (Second Edition)*, **2015**, 73-88.
- [24] J.Y. Qian, X.J. Li, Z.X. Gao, Z.J. Jin, Mixing efficiency and pressure drop analysis of liquid-liquid two phases flow in serpentine microchannels, *Journal of Flow Chemistry*, **2019**, 9(3), 187-197.
- [25] C.W. Pinger, A.A. Heller, D.M. Spence, A Printed Equilibrium Dialysis Device with Integrated Membranes for Improved Binding Affinity Measurements, *Analytical Chemistry*, **2017**, 89(14), 7302-7306.
- [26] B. Kasetsoontorn, N. Choengchan, Towards direct analysis of solid and liquid samples exploiting a 3D printed dialysis unit and sequential injection: Application for automated derivatization and determination of gamma-aminobutyric acid in foodstuff and beverages, *Analytica Chimica Acta*, **2020**, 1097 103-109.
- [27] H.A. Liebhafsky, H.G. Pfeiffer, Beer's law in analytical chemistry, *Journal of Chemical Education*, **1953**, 30(9), 450.
- [28] W. Laiwattanapaisa, T. Songjaroen, T. Maturos, T. Lomas, A. Sappat, A. Tuantranont, On-Chip Immunoassay for Determination of Urinary Albumin, *Sensors (14248220)*, **2009**, 9(12), 10066-10079.
- [29] J.S. Velazquez-Gonzalez, D. Monzon-Hernandez, F. Martinez-Pinon, D.A. May-Arrioja, I. Hernandez-Romano, Surface Plasmon Resonance-Based Optical Fiber Embedded in PDMS for Temperature Sensing, *Ieee Journal of Selected Topics in Quantum Electronics*, **2017**, 23(2), 6.
- [30] L.J. Golonka, H. Roguszcak, T. Zawada, J. Radojewski, I. Grabowska, M. Chudy, A. Dybko, Z. Brzozka, D. Stadnik, LTCC based microfluidic system with optical detection, *Sensors and Actuators B-Chemical*, **2005**, 111 396-402.
- [31] C.P. Chen, A.D. Townsend, E.A. Hayter, H.M. Birk, S.A. Sell, R.S. Martin, Insert-based microfluidics for 3D cell culture with analysis, *Analytical and Bioanalytical Chemistry*, **2018**, 410(12), 3025-3035.